



MA_4Ir_2 ($M = Ca, Sr, Eu$): superstructures of the KAu_4In_2 type

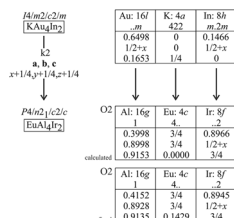
Nazar Zaremba^{1,2,3} · Volodymyr Pavlyuk^{1,4} · Frank Stegemann^{3,5} · Viktor Hlukhyy³ · Stefan Engel⁶ · Steffen Klenner⁵ · Rainer Pöttgen⁵ · Oliver Janka^{5,6} 

Received: 17 August 2022 / Accepted: 7 November 2022 / Published online: 21 December 2022
© The Author(s) 2022

Abstract

Three new iridium aluminum intermetallics $CaAl_4Ir_2$, $SrAl_4Ir_2$, and $EuAl_4Ir_2$ were synthesized from the elements using silica or tantalum ampoules. They crystallize in the tetragonal crystal system with space group $P4/ncc$ and lattice parameters of $a = 782.20(1)$ and $c = 779.14(2)$ pm for $CaAl_4Ir_2$, $a = 797.62(1)$ and $c = 772.75(2)$ pm for $SrAl_4Ir_2$, and finally $a = 791.78(5)$ and $c = 773.31(5)$ pm for $EuAl_4Ir_2$. All compounds crystallize isostructurally and adopt a new structure type that can be derived from the KAu_4In_2 type structure. To compare the structures from a crystallographic point of view, a group–subgroup relation between KAu_4In_2 and $EuAl_4Ir_2$ as well as KAu_4In_2 and KAu_4Sn_2 have been established using the Bärnighausen formalism. Finally, quantum-chemical calculations have been conducted, showing that in all three title compounds, a polyanionic $[Al_4Ir_2]^{\delta-}$ network exists with significant (polar) bonding interactions, while the respective $Ca^{\delta+}$, $Sr^{\delta+}$, and $Eu^{\delta+}$ cations are located in octagonal channels.

Graphical abstract



Keywords Crystal structure · Alkaline earth · Europium · Iridium · Aluminum · Intermetallics

✉ Oliver Janka
oliver.janka@uni-saarland.de

- ¹ Department of Analytical Chemistry, Ivan Franko National University of Lviv, Kyryla I Mefodiya Street 6, Lviv 79005, Ukraine
- ² Max-Planck-Institut für Chemische Physik fester Stoffe, Chemische Metallkunde, Nöthnitzer Straße 40, 01187 Dresden, Germany
- ³ Department of Chemistry, Technische Universität München, Lichtenbergstrasse 4, 85747 Garching, Germany
- ⁴ Institute of Chemistry, Częstochowa Jan Długosz University in Częstochowa, Al. Armii Krajowej 13/15, 42200 Częstochowa, Poland
- ⁵ Institut für Anorganische und Analytische Chemie, Westfälische Wilhelms-Universität Münster, Corrensstrasse 30, 48149 Münster, Germany
- ⁶ Universität des Saarlandes, Anorganische Festkörperchemie, Campus C4 1, 66123, Saarbrücken, Germany

Introduction

The rare earth (RE) and transition metals (T) form numerous ternary intermetallic compounds with aluminum [1]. Besides fundamental research with respect to phase analyses and determination of isothermal sections of the $RE-T-Al$ phase diagrams, these $RE_xT_yAl_z$ phases are of interest with respect to their broadly varying crystal chemistry and magnetic properties. Many of these phases find, e.g., application as precipitation hardening in modern light-weight aluminum-based alloys [2]. Usually, the rare earth elements are in a stable trivalent oxidation state. Europium, in contrast, prefers the stable divalent state due to a half-filled 4f shell with an electron configuration of $[Xe] 4f^7$. It is, thus, isoelectronic with Gd^{3+} and exhibits a high magnetic moment of $7.94 \mu_B$ per Eu/Gd atom, a good prerequisite for interesting

magnetic properties. However, so far, no complete isothermal section of the Eu–*T*–Al systems was studied. The only work is the partial section from 0 to 33.3 at% Eu for the Eu–Ag–Al system [3]. In view of the magnetic properties, representative examples are the antiferromagnets EuTi₂Al₂₀ ($T_N = 3.6$ K) and EuV₂Al₂₀ ($T_N = 5.5$ K) [4] and the quaternary silicides EuRhAl₄Si₂ ($T_C = 11$ K) and EuIrAl₄Si₂ ($T_C = 15$ K) [5].

When it comes to the 5d metals, the information is scarce. Only the Eu–Au–Al system was studied in some more detail and the compounds were reported: equiatomic EuAuAl which orders antiferromagnetically at $T_C = 50$ K [6], EuAu_{6.09}Al_{5.91} which structurally derives from the NaZn₁₃ type [7], EuAuAl₃ [8], Eu₂Au₆Al₃ [9], EuAu_{4.82}Al_{2.18} [7], EuAu₂Al₂ [10, 11], and the $T_C = 16.5$ K ferromagnet EuAu₃Al₂ [12].

In contrast, hardly any compounds were reported for the ternary systems with *T* = Os, Ir, and Pt [1]; however, recent phase analytical studies revealed highly interesting results with respect to new compounds. MgCuAl₂ type EuPtAl₂ orders ferromagnetically at $T_C = 54$ K [13] and an abrupt valence change at $T \sim 45$ K was observed in Eu₂Pt₆Al₁₅ [14]. A really remarkable compound is Eu₂Ir₃Al₉ [15], one of the rare examples of an intermetallic phase with purely trivalent europium.

The synthesis of such europium-based intermetallic phases deserves careful reaction conditions, since europium metal has a comparatively low boiling temperature of only 1870 K [16]. Some syntheses were conducted in quasi-open arc-melting furnaces (e.g., for EuAu₂Al₂ [11]), leading to europium evaporation, and thus changes of the initial sample composition. Better results can be obtained in sealed high-melting metal ampoules (niobium or tantalum, e. g., for Eu₂Au₆Al₃ [9]) or by synthesis in a low-melting metal flux (e.g., for EuIrAl₄Si₂ [5]). In the case of low Eu-content compounds, the constituent elements can be wrapped in Al foil and carefully arc melted (Eu₂Pt₆Al₁₅ [14]).

In the course of our systematic phase analytical work in the Eu–*T*–Al systems with the 5d metals, EuAl₄Ir₂ could be obtained. Synthetic attempts to obtain isostructural alkaline earth representatives yielded also CaAl₄Ir₂ and SrAl₄Ir₂. Herein, we report on their crystal chemistry and the structural relationship with the aristotype KAu₄In₂ [17].

Results and discussion

Phase analysis

Synthetic attempts to yield phase pure samples of CaAl₄Ir₂ (82(1) wt.-%) resulted in the formation of the title phases along with binary IrAl (11(1) wt.-%) and Ca₂Ir₃Al₉ (7(1) wt.-%), in the case SrAl₄Ir₂ (80(1) wt.-%), IrAl (20(1)

wt.-%) and traces of a yet unidentified phase were observed. Weight fractions were obtained by Rietveld refinement. For EuAl₄Ir₂, only traces of the title compound could be observed, the main product was Eu₂Ir₃Al₉ along with binary IrAl. When comparing the product composition with the weighed rations, it becomes evident that Ca/Sr is lost. This can often be found in the lid of the refractory metal ampoules; however, even an excess of alkaline-earth metal does not enable the synthesis of phase pure samples.

Crystal chemistry

EuAl₄Ir₂, CaAl₄Ir₂, and SrAl₄Ir₂ crystallize with a new structure type, in the tetragonal crystal system with space group *P4/ncc*, Pearson symbol *tP28* and Wyckoff sequence *gfc*. A view of the EuAl₄Ir₂ structure along the *c* axis is presented in Fig. 1. Each iridium atom is coordinated by eight aluminum atoms in the shape of a bicapped trigonal prism with Ir–Al distances ranging from 253 to 275 pm, the shortest distances found in the structure. These distances are a bit longer than the sum of the covalent radii [16] of 251 pm for Ir + Al. In addition, homoatomic Al–Al interactions can be observed (vide infra). Therefore, both the Ir–Al and Al–Al contacts can be considered bonding interactions with the iridium and aluminum atoms building an [Al₄Ir₂]^{δ-} network, which leaves large channels (eight-membered rings) that are filled by the europium atoms. The Eu–Ir and Eu–Al distances are 316 pm and range from 321 to 354 pm, which are slightly to well above the sum of the covalent radii (Eu + Ir = 311 pm / Eu + Al = 310 pm) suggesting rather weak bonding interactions.

The structural motif readily reminds of the KAu₄In₂ structure [17] and its isotypic compounds RbAu₄In₂ [17], CaNi₄Sn₂ [18], SrNi₄Sn₂ [18], SrCu₄Sn₂ [19], and EuCu₄Sn₂ [20]. The KAu₄In₂ type structure [17], however, crystallizes with the body centered space group *I4/mcm*. Consequently, EuAl₄Ir₂ could be a superstructure variant of KAu₄In₂. The corresponding group–subgroup scheme, proving their direct relationship, is shown in Fig. 2 using the Bärnighausen formalism [21–25]. Space group *P4/ncc* is a *klassengleiche* subgroup of index 2 of *I4/mcm*.

The main shift in the atomic parameters in the lower symmetric EuAl₄Ir₂ structure concerns the europium atoms. The inverse coloring of the transition metal and *p* element positions in the pair KAu₄In₂ / EuAl₄Ir₂ leads to a significantly different bonding situation, resulting in a shift of the europium atoms off the subcell mirror plane. For the aluminum position a decoupling of the *x* and *y* parameters is observed. These displacements allow for (i) the adjustment of the different size of the transition metal and the *p* element and (ii) an optimized bonding of europium with the network.

Figure 3 presents cutouts of the channels (eight-membered rings) of the KAu₄In₂ and EuAl₄Ir₂ structures.

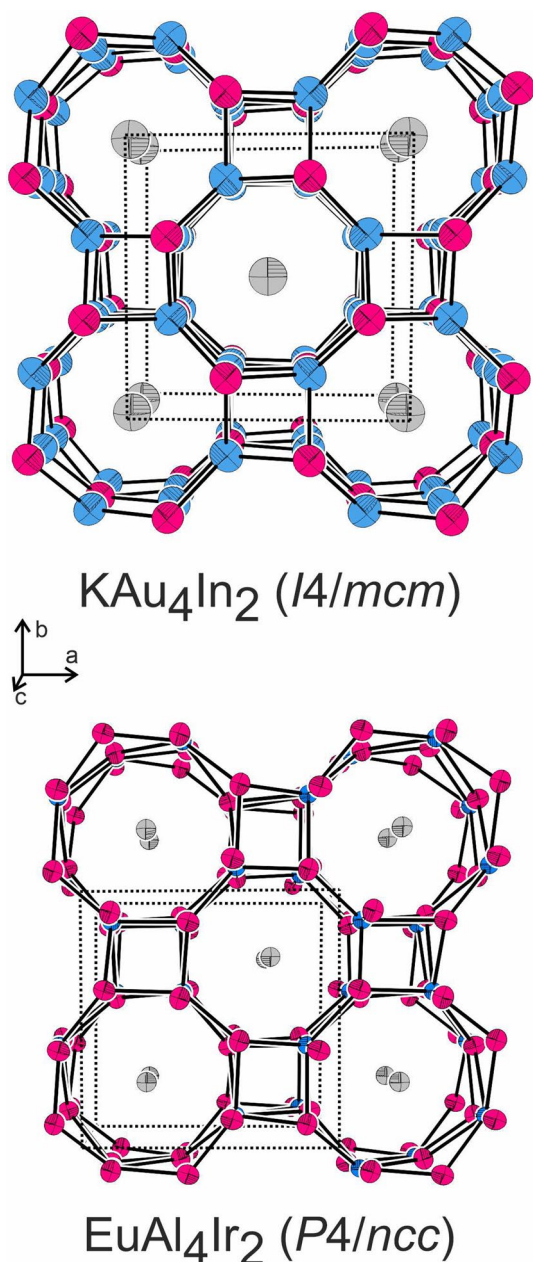


Fig. 1 View of the KA₄In₂ [17] and EuAl₄Ir₂ structures along the *c* axes. Potassium (europium), gold (iridium), and indium (aluminum) atoms are drawn as medium gray, blue, and magenta circles, respectively. Displacement ellipsoids are drawn at a 99% level. The [Au₄In₂]⁶⁻ and [Al₄Ir₂]⁶⁻ networks are emphasized

Although the transition metals are the most electronegative elements in both compounds (Au: 2.54 and Ir: 2.20 on the Pauling scale [16] vs. In: 1.78 and Al 1.61), we observe the inverse coloring of the polyanion. Another striking point is the charge difference between K⁺ and Eu²⁺. In KA₄In₂, the potassium atoms are located on mirror planes perpendicular to the *c* axis and are coordinated by eight gold atoms (338 pm K–Au). The coordination shell is enhanced by eight

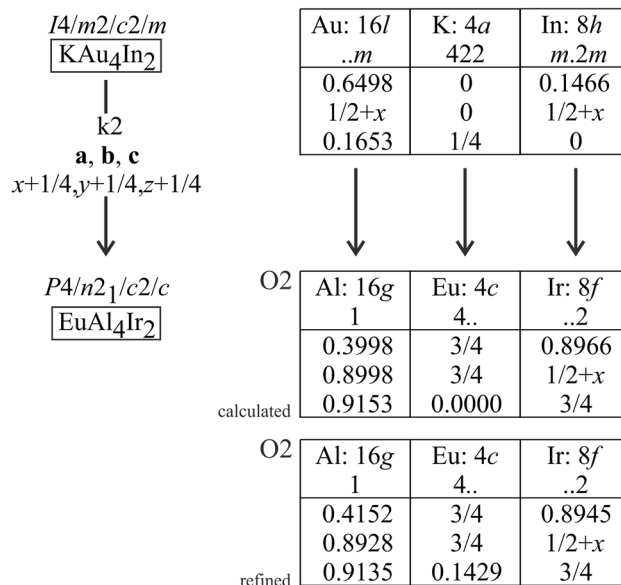


Fig. 2 Group-subgroup scheme in the Bärnighausen formalism [21–25] for the structures of KA₄In₂ [17] and EuAl₄Ir₂. The index for the *klassengleiche* (*k*) symmetry reduction, the origin shift and the evolution of the atomic parameters are given. Note that the EuAl₄Ir₂ structure is described in the setting O2

indium atoms at the much longer K–In distances of 392 pm. The situation is different in EuAl₄Ir₂. As a consequence of the exchanges of Au → Al and In → Ir the europium atoms shift in *c* direction and are coordinated by four iridium (316 pm) and twelve aluminum (321–354 pm) neighbors (Fig. 4, left). The different cation coordination can be considered as a kind of puckering effect for bond maximization.

CaAl₄Ir₂ and SrAl₄Ir₂ exhibit smaller / larger unit cells compared to EuAl₄Ir₂ (see Table 1), in line with the differing ionic radii (ionic radius Ca²⁺: 112, Sr²⁺: 126 pm, Eu²⁺: 125 pm, all CN=8 [26]). Therefore, displacements of the Ca / Sr atoms are observed; however, only small variations in the Ir and Al positions take place (Table 2). Since Ca²⁺ is slightly smaller compared to Eu²⁺ shorter Ca–Ir (307 pm) and Ca–Al (319–345 pm) distances are found nicely underlining the geometric influence of the cation in the cavities. In contrast, the Sr–Ir (317 pm) and Sr–Al (323–355 pm) distances are a bit elongated (Table 3), in line with the slightly larger ionic radius.

This geometric consideration is nicely underpinned by another closely related crystal structure. The stannide KA₄Sn₂ reported by Sinnen and Schuster [27] crystallizes in the non-centrosymmetric space group *I4̄c2*. The latter is a *translationengleiche* subgroup of *I4/mcm*. The underlying group-subgroup scheme is shown in Fig. 5. KA₄Sn₂ keeps a body-centered lattice; however, similar to the EuAl₄Ir₂ structure, a decoupling of the *x* and *y* parameters on the 16i site takes place. This way, the gold atoms can react on the

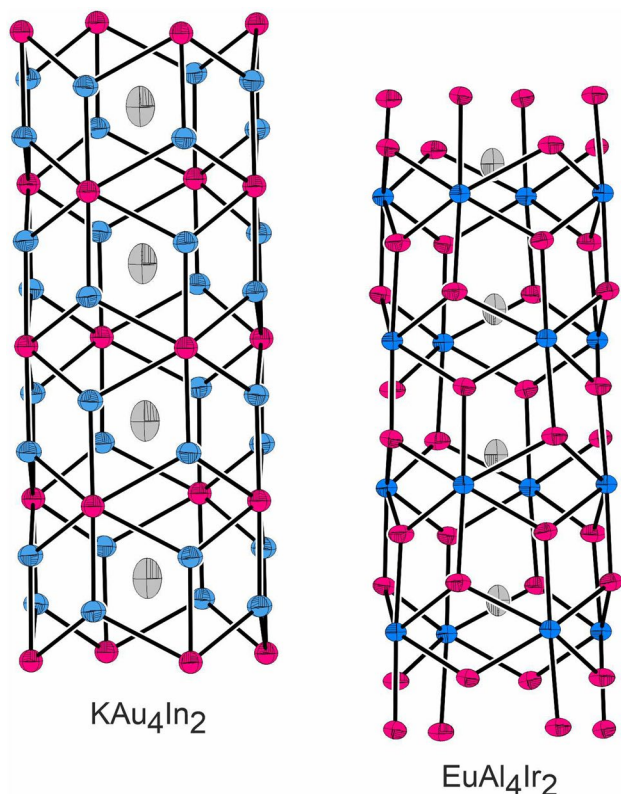


Fig. 3 Cutout of the channels (eight-membered rings) in the structures of KAu_4In_2 [17] and EuAl_4Ir_2 . Potassium (europium), gold (iridium), and indium (aluminum) atoms are drawn as medium gray, blue, and magenta circles, respectively. Displacement ellipsoids are drawn at an 80% level for KAu_4In_2 and at 99% for EuAl_4Ir_2

slightly smaller size (covalent radius 139 pm [16]) of the tin atoms as compared to indium (covalent radius 142 pm [16]). The distortions in KAu_4Sn_2 are much more subtle compared to EuAl_4Ir_2 .

Finally, we draw back to the $[\text{Al}_4\text{Ir}_2]^{\delta-}$ network in the EuAl_4Ir_2 structure. Besides substantial Ir–Al bonding, we

observe a range of Al–Al homoatomic interactions with Al–Al distances of 255–273 pm, all shorter than in *fcc* aluminum (12×286 pm [28]) but slightly longer than the sum of the covalent radii (250 pm) [16]. These interactions substantially stabilize the EuAl_4Ir_2 structure. We address these features in more detail in the following chapter on the basis of electronic structure calculations.

The valence electron count (VEC) in contrast is not simple to discuss. It increases from SrNi_4Sn_2 (VEC = 50), via KAu_4In_2 (VEC = 51) and KAu_4Sn_2 (VEC = 53) to SrCu_4Sn_2 (VEC = 54). With the inverse coloring for EuAl_4Ir_2 the VEC has the much lower value of 32, underpinning the different bonding situation.

Electronic structure calculations

The experimental crystallographic data obtained in this work was used for electronic structure calculations. The performed calculations of the electronic structure confirm the existence of an $[\text{Al}_4\text{Ir}_2]$ network in all three phases. Higher electron localization (red regions) is observed around the Al and Ir atoms, which are the most electronegative component (Fig. 6) compared to Ca, Sr, or Eu which donate their valence electrons. However, it should be noted, that the values of the maxima of the electronic localization functions (ELF) are somewhat different, in particular ELF = 0.863 (for CaAl_4Ir_2), 0.740 (for SrAl_4Ir_2), and 0.655 (for EuAl_4Ir_2), respectively. The alkaline earth metals (Ca and Sr) donate their valence electrons more easily than the rare earth metal europium. The ELF iso-surfaces presented in Fig. 6 suggest that polyatomic network is partially negatively charged according to $[\text{Al}_4\text{Ir}_2]^{\delta-}$ that is compensated by positively charged alkaline earth or rare earth metals.

These results are in line with the electronegativities ($\chi(\text{Ca}) = 1.00$; $\chi(\text{Sr}) = 0.95$; $\chi(\text{Eu}) = 1.2$; $\chi(\text{Al}) = 1.61$; $\chi(\text{Ir}) = 2.20$ [16]) and are confirmed by Bader charges calculated for $\text{Ca}_2\text{Ir}_3\text{Al}_9$ [29].

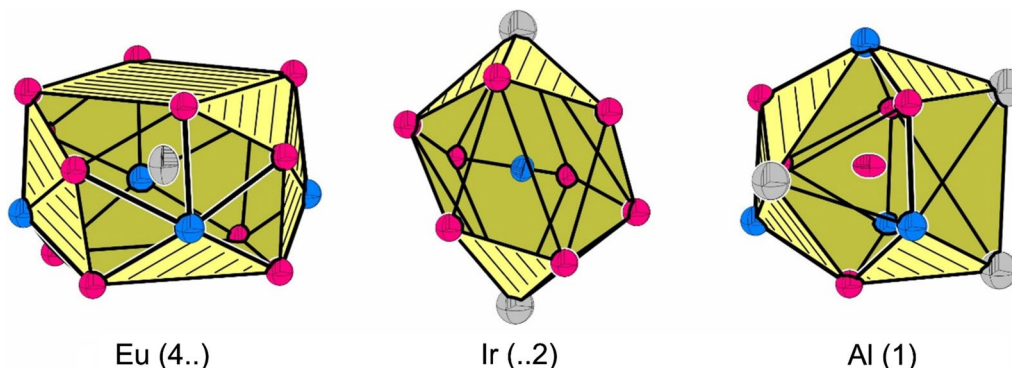


Fig. 4 Coordination polyhedra surrounding the Eu (left), Ir (middle), and Al (right) atoms in the structure of EuAl_4Ir_2 . Europium, iridium, and aluminum atoms are drawn as medium gray, blue, and magenta circles, respectively. The site symmetries are given

Table 1 Crystallographic data and structure refinement details for CaAl₄Ir₂, SrAl₄Ir₂, and EuAl₄Ir₂, space group *P4/ncc*, Z=4

Empirical formula	CaAl ₄ Ir ₂	SrAl ₄ Ir ₂	EuAl ₄ Ir ₂
CCDC number	2182278	2182277	2182276
Lattice parameters			
Powder/pm	<i>a</i> = 782.20(1) <i>c</i> = 779.14(2)	797.62(1) 772.75(2)	– –
Cell volume/nm ³	<i>V</i> = 0.4767	0.4916	–
Single crystal/pm	<i>a</i> = 781.56(6) <i>c</i> = 778.65(7)	796.13(6) 771.57(7)	791.81(5) 773.31(5)
Cell volume/nm ³	<i>V</i> = 0.4756	0.4980	0.4848
Molar mass/g mol ⁻¹	532.4	580.0	644.3
Calculated density/g cm ⁻³	7.44	7.88	8.83
Crystal size/μm ³	36 × 62 × 75	40 × 60 × 50	80 × 80 × 160
Diffractometer type	IPDS-II (Stoe)	Bruker APEX-II	IPDS-II (Stoe)
Detector distance/mm	70	40	70
Exposure time/min	15	0.25	5
<i>ω</i> -range/step width/deg	0–180/1.0	–/0.5	0–180/1.0
Integr. Param. A, B, EMS	15.0, 4.0, 0.010	–	15.0, –2.0, 0.020
Absorption coefficient/mm ⁻¹	57.5	65.7	68.1
<i>F</i> (000)/ <i>e</i>	904	976	1076
<i>θ</i> range/deg	3.69–33.39	3.62–31.78	3.64–33.35
<i>hkl</i> range	–12, +11; –12, +11; –11, +10	± 10, ± 11, –11, +11;	± 12, ± 12, ± 11
Total no. reflections	6951	4042	5728
Independent reflections/ <i>R</i> _{int}	461/0.0408	399/0.0304	474/0.0530
Refl. with <i>I</i> ≥ 3σ(<i>I</i>)/ <i>R</i> _σ	281/0.0144	341/0.0169	407/0.00052
Data/parameters	461/19	399/19	474/19
Goodness-of-fit on <i>F</i> ²	0.95	1.23	2.10
<i>R</i> ₁ / <i>wR</i> ₂ for <i>I</i> ≥ 3σ(<i>I</i>)	0.0125/0.0408	0.0201/0.0155	0.0235/0.0548
<i>R</i> ₁ / <i>wR</i> ₂ for all data	0.0255/0.0342	0.0418/0.0401	0.0302/0.0560
Extinction coefficient	129(9)	149(13)	460(30)
Largest diff. peak/hole/e Å ⁻³	+2.69/–3.69	+1.40/–1.20	+3.26/–2.56

Table 2 Atomic coordinates and displacement parameters [pm²] for CaAl₄Ir₂, SrAl₄Ir₂, and EuAl₄Ir₂ (space group *P4/ncc*, Z=4)

Atom	Wyck	<i>x</i>	<i>y</i>	<i>z</i>	<i>U</i> ₁₁	<i>U</i> ₂₂	<i>U</i> ₃₃	<i>U</i> ₁₂	<i>U</i> ₁₃	<i>U</i> ₂₃	<i>U</i> _{eq}
CaAl ₄ Ir ₂											
Ca	4 <i>c</i>	3/4	3/4	0.1671(3)	89(2)	<i>U</i> ₁₁	179(11)	0	0	0	119(4)
Ir	8 <i>f</i>	0.89311(2)	1/2 + <i>x</i>	3/4	66(1)	<i>U</i> ₁₁	63(1)	–1(1)	1(1)	–1(1)	65(1)
Al	16 <i>g</i>	0.4146(2)	0.8850(2)	0.9136(2)	97(7)	84(7)	80(6)	–9(6)	4(5)	–2(6)	87(4)
SrAl ₄ Ir ₂											
Sr	4 <i>c</i>	3/4	3/4	0.14563(9)	51(2)	<i>U</i> ₁₁	121(4)	0	0	0	74(2)
Ir	8 <i>f</i>	0.89194(2)	1/2 + <i>x</i>	3/4	41(1)	<i>U</i> ₁₁	32(2)	1(1)	0(1)	0(1)	38(1)
Al	16 <i>g</i>	0.4140(2)	0.8838(2)	0.9137(2)	70(6)	53(3)	40(8)	–10(4)	–4(5)	–1(5)	54(4)
EuAl ₄ Ir ₂											
Eu	4 <i>c</i>	3/4	3/4	0.14287(7)	82(2)	<i>U</i> ₁₁	180(3)	0	0	0	104(1)
Ir	8 <i>f</i>	0.89249(3)	1/2 + <i>x</i>	3/4	69(1)	<i>U</i> ₁₁	54(2)	0(1)	0(1)	0(1)	64(1)
Al	16 <i>g</i>	0.4152(3)	0.8835(2)	0.9134(3)	103(7)	88(7)	51(9)	–6(6)	–3(6)	–2(6)	79(5)

The equivalent isotropic displacement parameter *U*_{eq} is defined as *U*_{eq} = 1/3 (*U*₁₁ + *U*₂₂ + *U*₃₃) (pm²). Coefficients *U*_{ij} of the anisotropic displacement factor tensor of the atoms are defined by: $-2\pi^2[(ha^*)^2U_{11} + \dots + 2hka^*b^*U_{12}]$. Standard deviations are given in parentheses

Table 3 Interatomic distances (pm) for CaAl_4Ir_2 , SrAl_4Ir_2 , and EuAl_4Ir_2

Ca	4	Ir	307.4	Al	1	Ir	252.5	
	4	Al	319.2		1	Al	256.8	
	4	Al	341.6		1	Al	261.2	
	4	Al	344.7		1	Ir	262.4	
	2	Ca	389.3		1	Ir	262.6	
	Ir	2	Al	252.5		2	Al	271.1
		2	Al	262.4		1	Ir	272.2
		2	Al	262.6		1	Ca	319.2
		2	Al	272.2		1	Ca	341.6
		2	Ca	307.4		1	Ca	344.7
Sr		4	Ir	317.0	Al	1	Ir	253.9
	4	Al	322.7		1	Al	254.9	
	4	Al	339.0		1	Ir	260.1	
	4	Al	354.5		1	Al	265.9	
	2	Sr	385.8		1	Ir	267.7	
	Ir	2	Al	253.9		2	Al	273.0
		2	Al	260.1		1	Ir	274.5
		2	Al	267.7		1	Sr	322.7
		2	Al	274.5		1	Sr	339.0
		2	Sr	317.0		1	Sr	354.5
Eu		4	Ir	315.8	Al	1	Ir	253.2
	4	Al	321.2		1	Al	255.3	
	4	Al	336.0		1	Al	260.9	
	4	Al	353.9		1	Ir	264.4	
	2	Eu	386.7		1	Ir	265.7	
	Ir	2	Al	253.2		2	Al	272.9
		2	Al	260.9		1	Ir	274.6
		2	Al	265.7		1	Eu	321.2
		2	Al	274.6		1	Eu	336.0
		2	Eu	315.8		1	Eu	353.9

Standard deviations are equal or smaller than 0.1 pm. All distances of the first coordination spheres are listed

The integrated crystal orbital Hamilton population ($-i\text{COHP}$) values confirm that the strongest bonding is between the aluminum and iridium atoms. For the Ir–Al bond the $-i\text{COHP}$ values are 2.317 eV (for CaAl_4Ir_2), 2.141 eV (for SrAl_4Ir_2), and 2.093 eV (for EuAl_4Ir_2), respectively. For the homoatomic Al–Al bonds, the $-i\text{COHP}$ values are much smaller, almost by a factor of two.

The total and partial densities of states (DOS) for all structures are shown in Fig. 7. For EuAl_4Ir_2 , the 4f orbitals were taken into calculations which give the locations of the occupied and unoccupied 4f states to be -6 and 3.8 eV with respect to E_F , respectively. In Fig. 7, the Eu partial DOS consists of a corresponding large peak at 3.8 eV and a small but broadened peak -6 eV (extend from -5 to -7 eV). Visible density of electronic states at the Fermi level for these compounds indicates metallic behavior. A common feature of these kind of structures is a very intense peak due to the overlap of the d-orbital of Ir and the p-orbitals of Al in the valence band between -2 to -4 eV (for CaAl_4Ir_2 and SrAl_4Ir_2). For EuAl_4Ir_2 , the significant shift of Ir-5d states up

to a range from -5 to -7 eV compared to the range from -2 to -4 eV in the Ca- and Sr-compounds is obviously caused by the presence of additional interactions of the electrons of the occupied 5d orbital of iridium with the electrons of the occupied 4f orbital of europium, the states of which are actually in the interval from -5 to -7 eV.

Conclusion

CaAl_4Ir_2 , SrAl_4Ir_2 , and EuAl_4Ir_2 could be synthesized from the elements and were characterized via single crystal and powder X-ray diffraction experiments. They all crystallize with space group $P4/ncc$ and adopt a new structure type which can be derived from the KAu_4In_2 type structure ($I4/mcm$). The title compounds, however, exhibit an inverse coloring of the $[\text{Al}_4\text{Ir}_2]^{\delta-}$ network with significant polar bonding interactions. Within the polyanion, octagonal channels are observed that host the $\text{Ca}^{\delta+}$, $\text{Sr}^{\delta+}$, and $\text{Eu}^{\delta+}$ cations. The structural relation was established using a

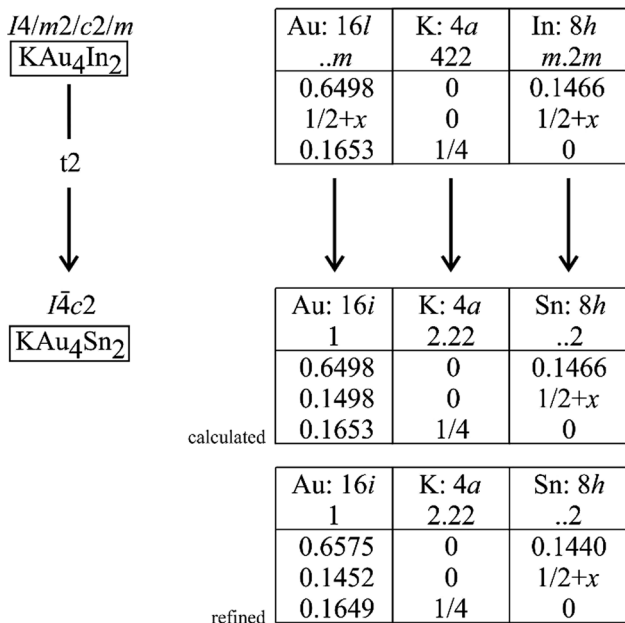


Fig. 5 Group–subgroup scheme in the Bärnighausen formalism [21–25] for the structures of KAu₄In₂ [17] and KAu₄Sn₂ [27]. The index for the *translationengleiche* (*t*) symmetry reduction and the evolution of the atomic parameters are given

group-subgroup scheme. Analysis of the electronic localization function shows, that the proposed network in all three title compounds exhibits a significant negative charge, with larger absolute charges for the alkaline earth compounds, in line with their lower electronegativities.

Experimental

Synthesis

Starting materials for the synthesis of the samples were europium ingots (American Elements, 99.99%), calcium and strontium pieces (Alfa Aesar, 99.9%), iridium powder (Agosi, 99.9%), and aluminum turnings (Koch Chemicals, 99.9%). For the synthesis of EuAl₄Ir₂, the elements were initially weighed in the atomic ratio 1:2:1 and sealed in an evacuated silica ampoule. The latter was placed in a muffle furnace, heated to 1373 K, kept at that temperature for 6 h, followed by rapid cooling to 873 K and a further annealing step at that temperature for 240 h.

For CaAl₄Ir₂ and SrAl₄Ir₂, the constituent metals were also used in their elemental form and weighed in the ideal stoichiometric ratios. Pieces of the elements were loaded into

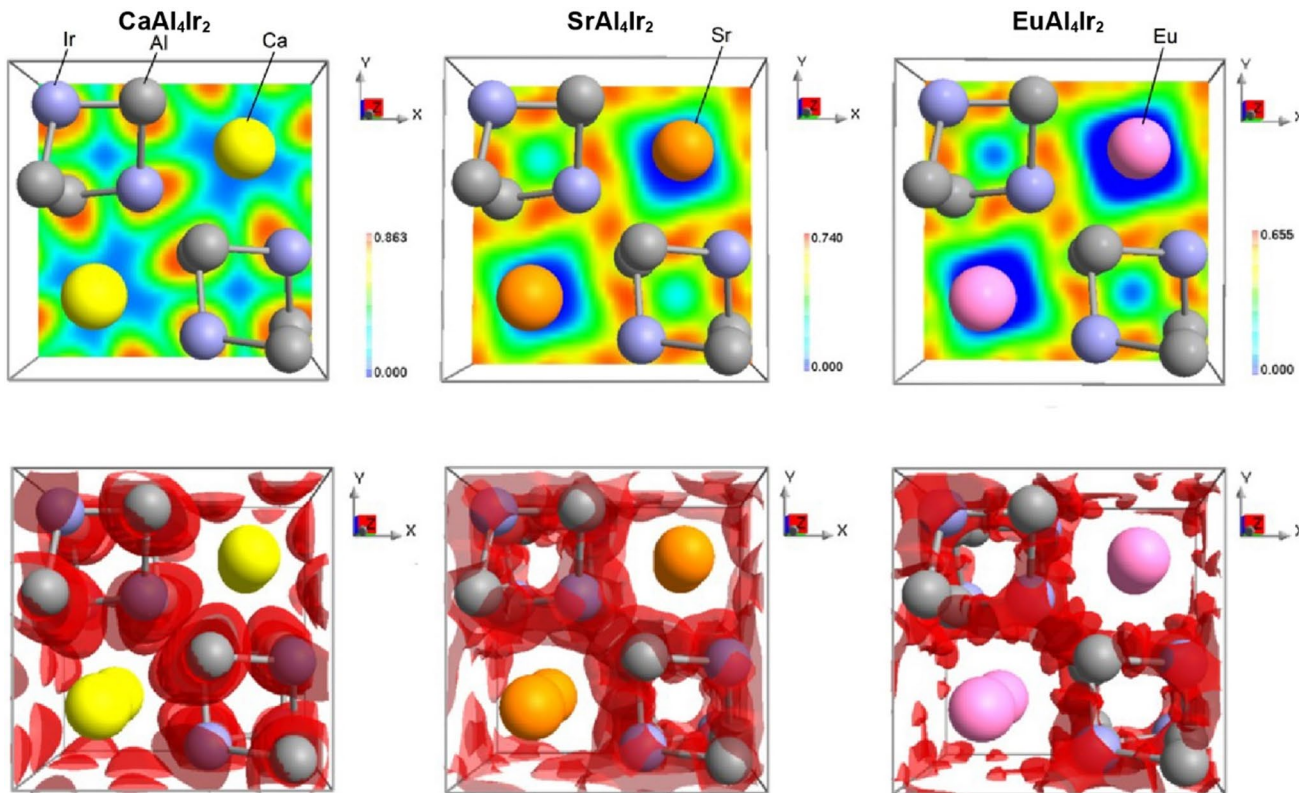


Fig. 6 Electron localization function (ELF) mapping around the particular atoms in CaAl₄Ir₂, SrAl₄Ir₂, and EuAl₄Ir₂ (top) and iso-surfaces of ELF (bottom). The isosurfaces of ELF around the atoms for

all structures are drawn at the same levels: isosurface value is 75%, opacity value 70%

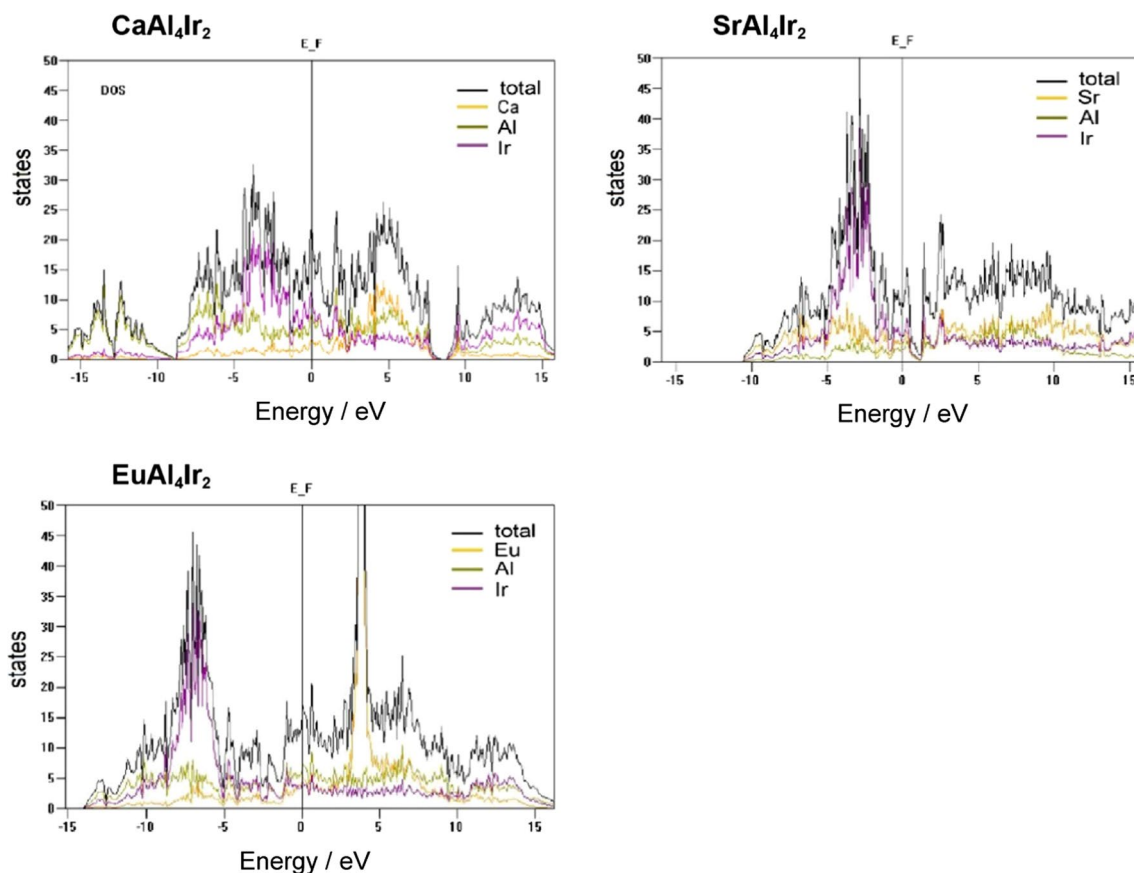


Fig. 7 Density of states in CaAl_4Ir_2 , SrAl_4Ir_2 , and EuAl_4Ir_2

tantalum tubes which were subsequently arc-welded [30] under an argon pressure of about 800 mbar. The argon gas was purified over titanium sponge (873 K), molecular sieves and silica gel. The respective alkaline earth metals and europium pieces were cleaned mechanically under dried (Na) cyclohexane and were kept in Schlenk tubes under argon prior to use. For sealing the ampoules, the elements were added to the tantalum tube in an argon counter-flow. The gas-tight sealed containers were then placed into the water-cooled reaction chamber of an induction furnace (Hüttinger Elektronik, type 1.5/300 or TRUMPF Hüttinger TruHeat HF 5010) and rapidly heated twice to about 1573 K for 20 min interrupted by switching off the power supply for one minute [31]. The temperature was controlled using a Sensor Therm Methis MS09 pyrometer with a stated accuracy of ± 50 K. The tantalum tubes were quenched; no reaction of the samples with the container material was observed.

EDX data

The single crystals of CaAl_4Ir_2 and EuAl_4Ir_2 , investigated on the diffractometer, were semiquantitatively analyzed by EDX in a Zeiss EVO® MA10 scanning electron microscope

(variable pressure mode (60 Pa) and W cathode) using CaF_2 , EuF_3 , Ir, and Al_2O_3 as standards (ZAF correction algorithm (Z = atomic number, A = absorption, F = fluorescence) in combination with fixed X-ray intensity values for the energies of the respective standards, the so-called standard-free analyses). The average of three point measurements on the irregular (conchoidal fracture) crystal surfaces of 16 ± 2 at.-% Ca: 29 ± 2 at.-% Ir: 55 ± 2 at.-% Al and 16 ± 2 at.-% Eu: 30 ± 2 at.-% Ir: 54 ± 2 at.-% Al confirm the ideal compositions (14.3 at.-% M: 28.6 at.-% Ir: 57.1 at.-% Al) refined from the single crystal X-ray data. No impurity elements heavier than sodium (detection limit of the instrument) were detected.

X-ray diffraction on powders and single crystals

To check the phase-purity, the polycrystalline samples of all samples were analyzed by powder X-ray diffraction: Guinier technique, image plate system Fujifilm, BAS-1800, Cu- $K\alpha_1$ radiation, and α -quartz ($a = 491.30$ pm, $c = 540.46$ pm) as an internal standard.

Powder X-ray diffraction (PXRD) patterns of the pulverized samples used for Rietveld refinements were recorded

at room temperature on a D8-A25-Advance diffractometer (Bruker, Karlsruhe, Germany) in Bragg–Brentano θ – θ -geometry (goniometer radius 280 mm) with Cu K α radiation ($\lambda = 154.0596$ pm). A 12 μ m Ni foil working as K β filter and a variable divergence slit were mounted at the primary beam side. A LYNXEYE detector with 192 channels was used at the secondary beam side. Experiments were carried out in a 2θ range of 6–130° with a step size of 0.013° and a total scan time of 1 h. The recorded data was evaluated using the Bruker TOPAS 5.0 software [32], with the observed reflections being treated via single-line fits.

Irregularly shaped crystal splinters were selected from the crushed annealed samples and glued to glass fibers with beeswax. For a first-quality check, Laue patterns were collected on a Buerger precession camera (white Mo radiation, Fuji-film imaging plate). Complete data sets of suitable crystals were recorded at room temperature using a Stoe IPDS-II image plate system (graphite monochromatized Mo radiation; $\lambda = 71.073$ pm) in oscillation mode. A numerical absorption correction was applied to the data sets. Details on the crystallographic data are summarized in Table 1.

Structure refinements

The data sets showed a primitive tetragonal lattice with high Laue symmetry. Careful examination of the systematic extinctions revealed compatibility with space group $P4/ncc$ or its subgroups. The centrosymmetric group $P4/ncc$ was found to be correct. The starting atomic parameters were deduced with the charge flipping algorithm (program Superflip [33]) and the structures of CaAl₄Ir₂, SrAl₄Ir₂, and EuAl₄Ir₂ were refined by least squares on F^2 using the program Jana 2006 [34] with anisotropic displacement parameters for all atoms. For the final refinement cycles the atomic coordinates were transformed to the setting listed in the Bärnighausen tree. As a check for the correct compositions, the occupancy parameters of all sites were refined in separate series of least-squares cycles. All sites were fully occupied within two standard deviations. The final difference Fourier syntheses was contour-less. The refined atomic coordinates, displacement parameters and interatomic distances are listed in Tables 2 and 3.

CCDCs 2182276 (EuAl₄Ir₂), 2182277 (SrAl₄Ir₂), and 2182278 (CaAl₄Ir₂) contain the supplementary crystallographic data for this paper. These data can be obtained free of charge from The Cambridge Crystallographic Data Centre via www.ccdc.cam.ac.uk/data_request/cif.

Theoretical studies

All calculations were conducted by means of the tight-binding linear muffin-tin orbital method in the atomic spheres approximation (TB–LMTO–ASA) [35–37]. The exchange

and correlation effects were accounted for in terms of the local density approximation (LDA) [38]. The density of states (DOS) and the integrated crystal orbital Hamilton population (iCOHP) [39] values were used for chemical bonding analyses. The electron localization function (ELF) map was calculated as described in Ref. [40]. The visualization of electronic structure calculation data (ELF, DOS) was generated using the wxDragon program [41].

Acknowledgements This work was supported by the DAAD (Deutscher Akademischer Austauschdienst), grant no. 91619802. Instrumentation and technical assistance for this work were provided by the Service Center X-ray Diffraction, with financial support from Saarland University and German Science Foundation (project number INST 256/349-1). Funding has also been provided by the Deutsche Forschungsgemeinschaft DFG (JA 1891-10-1).

Funding Open Access funding enabled and organized by Projekt DEAL.

Open Access This article is licensed under a Creative Commons Attribution 4.0 International License, which permits use, sharing, adaptation, distribution and reproduction in any medium or format, as long as you give appropriate credit to the original author(s) and the source, provide a link to the Creative Commons licence, and indicate if changes were made. The images or other third party material in this article are included in the article's Creative Commons licence, unless indicated otherwise in a credit line to the material. If material is not included in the article's Creative Commons licence and your intended use is not permitted by statutory regulation or exceeds the permitted use, you will need to obtain permission directly from the copyright holder. To view a copy of this licence, visit <http://creativecommons.org/licenses/by/4.0/>.

References

- Villars P, Cenzual K (2020) Pearson's Crystal Data: Crystal Structure Database for Inorganic Compounds (release 2020/21). ASM International®, Materials Park, Ohio (USA)
- Kammer C (2001) Aluminium-Taschenbuch 1: Grundlagen und Werkstoffe, 16th edn. Beuth Verlag, Berlin
- Verbovytskyy Y, Pereira Gonçalves A (2013) Intermetallics 43:103
- Ramesh Kumar K, Nair HS, Christian R, Thamizhavel A, Strydom AM (2016) J Phys: Condens Matter 28:436002
- Maurya A, Thamizhavel A, Provino A, Pani M, Manfrinetti P, Paudyal D, Dhar SK (2014) Inorg Chem 53:1443
- Hulliger F (1993) J Alloys Compd 200:75
- Smetana V, Steinberg S, Mudryk Y, Pecharsky V, Miller GJ, Mudring A-V (2015) Inorg Chem 54:10296
- Hulliger F (1995) J Alloys Compd 218:255
- Gerke B, Pöttgen R (2014) Z Naturforsch 69b:121
- Hulliger F, Nissen H-U, Wessicken R (1994) J Alloys Compd 206:263
- Xue B, Hulliger F, Schwer H (1995) J Alloys Compd 221:L6
- Schmiegel J-P, Block T, Gerke B, Fickenscher T, Touzani RS, Fokwa BPT, Janka O (2016) Inorg Chem 55:9057
- Stegemann F, Block T, Klenner S, Zhang Y, Fokwa BPT, Timmer A, Mönig H, Doerenkamp C, Eckert H, Janka O (2019) Chem Eur J 25:10735
- Radzieowski M, Stegemann F, Block T, Stahl J, Johrendt D, Janka O (2018) J Am Chem Soc 140:8950

15. Stegemann F, Block T, Klenner S, Janka O (2019) *Chem Eur J* 25:3505
16. Emsley J (1999) *The Elements*. Oxford University Press, Oxford
17. Li B, Corbett JD (2006) *J Am Chem Soc* 128:12392
18. Hlukhyy V, Raif F, Claus P, Fässler TF (2008) *Chem Eur J* 14:3737
19. Pani M, Fornasini ML, Manfrinetti P, Merlo F (2011) *Intermetallics* 19:957
20. Mazzone D, Paulose PL, Dhar SK, Fornasini ML, Manfrinetti P (2008) *J Alloys Compd* 453:24
21. Bärnighausen H (1980) *Commun Math Chem* 9:139
22. Müller U (2004) *Z Anorg Allg Chem* 630:1519
23. Müller U (2010) *International Tables for Crystallography, Vol. A1, Symmetry relations between space groups*. John Wiley and Sons, Chichester, United Kingdom
24. Müller U (2012) *Symmetriebeziehungen zwischen verwandten Kristallstrukturen*. Vieweg + Teubner Verlag, Wiesbaden, Germany
25. Block T, Seidel S, Pöttgen R (2022) *Z Kristallogr* 237:215
26. Shannon RD, Prewitt CT (1969) *Acta Crystallogr B* 25:925
27. Sinnen H-D, Schuster U-U (1978) *Z Naturforsch* 33b:1077
28. Donohue J (1974) *The Structures of the Elements*. Wiley, New York
29. Stegemann F, Zhang Y, Fokwa BPT, Janka O (2020) *Dalton Trans* 49:6398
30. Pöttgen R, Gulden T, Simon A (1999) *GIT Labor-Fachz* 43:133
31. Pöttgen R, Lang A, Hoffmann R-D, Künnen B, Kotzyba G, Müllmann R, Mosel BD, Rosenhahn C (1999) *Z Kristallogr* 214:143
32. Bruker AXS Inc (2014) TOPAS 5.0, Karlsruhe, Germany
33. Palatinus L, Chapis G (2007) *J Appl Crystallogr* 40:786
34. Petříček V, Dušek M, Palatinus L (2014) *Z Kristallogr* 229:345
35. Andersen OK (1975) *Phys Rev B* 12:3060
36. Andersen OK, Jepsen O (1984) *Phys Rev Lett* 53:2571
37. Andersen OK, Pawłowska Z, Jepsen O (1986) *Phys Rev B* 34:5253
38. von Barth U, Hedin L (1972) *J Phys C* 5:1629
39. Dronskowski R, Blöchl PE (1993) *J Phys Chem* 97:8617
40. Becke AD, Edgecombe KE (1990) *J Chem Phys* 92:5397
41. Eck B (2103) wxDragon, RWTH Aachen, Aachen, Germany 2013

Publisher's Note Springer Nature remains neutral with regard to jurisdictional claims in published maps and institutional affiliations.